Crystallographic Characteristics of Nanostructured Thin-Film Fuel Cell Electrocatalysts: A HRTEM Study

Lajos Gancs,[†] Takeshi Kobayashi,[†] Mark K. Debe,*[,‡] Radoslav Atanasoski,[‡] and Andrzej Wieckowski*[,†]

Department of Chemistry, University of Illinois, 600 South Mathews Avenue, Urbana, Illinois, 61801, and Fuel Cell Components Program, 201-2N-19, 3M Center, 3M Company, St. Paul, Minnesota, 55144-1000

Received October 17, 2007. Revised Manuscript Received January 4, 2008

This paper reports a study of thin films of Pt and Pt-alloys deposited on oriented crystalline organic whiskers using high resolution transmission electron microscopy imaging. It is our opinion that these nanostructured thin film (NSTF) electrocatalysts are the leading electrode technology for polymer electrolyte fuel cells because of their significant advantages in durability and specific activity. The sputter-deposited thin catalyst films on the whiskers grow as polycrystalline layers that expose highly oriented fcc crystallites. Within the films, truncated pyramid-shaped crystallites grow into acicular whiskerettes on the whisker sides, and the whiskerette shapes display a growth mechanism governed by a strong support−metal interaction and surface energy minimization. The surface structure of the crystalline whiskers facilitates metal nucleation sites that are spaced evenly along the whisker length by ∼6–8 nm. The whiskerettes are the dominant structural form of the NSTF catalyst coatings at the loading levels investigated. Along just a few nanometers of a whisker's long axis, the whiskerettes can exhibit changes in aspect ratios up to a factor of 5 and thus may increase the surface roughness by a factor of 6. Diffractogram indexing suggests that the truncated pyramids expose four (111) and one (100) planes, which grow further into pillars by elongating their base along two of the (111) facets. When the atomic scale roughness is disregarded, the supported NSTF Pt-based electrocatalysts expose predominantly (111) facets.

I. Introduction

Environmental issues and national energy security have been the prominent drivers justifying research and development of alternative fuels and power sources for transportation. As the emerging market opportunity develops, current energy storage and conversion devices (such as batteries and internal combustion engines) are expected by some to be replaced over time with fuel cells. Fuel cell development over the last two decades, both low temperature (such as proton-exchange membrane) and high temperature (such as phosphoric acid), has triggered significant research activity in the field of heterogeneous electrocatalysis. While the most feasible half-cell reactions for oxygen reduction and hydrogen oxidation were proposed long ago and have been investigated in detail for years, many of the current research efforts concentrate on the improvement of the traditional electrocatalysts or on the development of novel electrode materials, particularly for oxygen reduction. To ensure acceptable reaction rates for the low-temperature electroreduction of molecular oxygen, precious metals, especially platinum, remain indispensable. Lowering the content of the expensive metals in fuel cells is one primary objective of the commercialization process. Improving electrodes, in general, translates to a higher utilization of the noble metals without sacrificing durability. Such strategies involve the development of three-dimensional, thin structures to facilitate mass transport that enable low concentration overpotentials and high electrocatalyst utilization. Employing alloys and tailoring surface morphology to obtain high area-specific activity are other major approaches. Furthermore, it is also important for high precious metal utilization to use supports and catalyst fabrication means that allow a high degree of dispersion of the electroactive compounds on the catalyst supports. Such general requirements stimulate the search for improved methods for the dispersion of noble metals and their alloys on inert, stable, and low-cost substrate materials.

Various types of rough or graphitized carbon powders constitute the most common type of support materials for current fuel-cell electrocatalyst applications. There are two main ways to prepare carbon-supported noble metal or metal alloy electrocatalysts:[1] (i) impregnation of the carbon powder with the precursor solution of the noble metal ions and (ii) adsorption of metal-oxides or colloids onto the carbon surface, each followed by reduction to the pure metallic form. Such processes expose small metal nanoparticles, which possess dynamically varying physical properties with typical dimensions on the scale of a few nanometers.[2] Correlating such variations to electrocatalytic activity has been an important motivation of the fuel-cell electrocatalysis research,

* To whom correspondence should be addressed. Phone: +1-217-333-7943 (A.W.); 651-736-9563 (M.K.D.). E-mail: andrzej@scs.uiuc.edu (A.W.); mkdebe1@mmm.com (M.K.D.).
[†] University of Illinois at Urbana-Champaign.
[‡] 3M Company.

(1) Antolini, E. *J. Mater. Sci.* **2003**, *38*, 2995.
(2) Santra, A. K.; Goodman, D. W. In *Catalysis and Electrocatalysis at Nanoparticle Surfaces*; Wieckowski, A., Savinova, E., Vayenas, C., Eds.; Decker: New York, 2003; p 281.

10.1021/cm702992b CCC: $40.75
Published on Web 03/07/2008

as reviewed in refs 2–4. In the case of nanoparticles in general, it is usually not the inadequacy of modern atomic-resolution microscopy and the spectroscopy techniques but the propensity of nanoparticles to undergo diverse surface faceting and the atomic-scale roughness that makes it difficult to draw reliable conclusions on how surface characteristics are related to activity. Although there are possibilities to tailor nanoparticle shapes and thereby surface faceting during preparation,[5] a high degree of uniformity in surface morphology and thus high reaction selectivity is not yet conveniently attainable.[1] The intrinsic instability of the nanoparticles, particularly in a fuel cell environment, also contributes to the complexity of the problem because the elemental composition, morphology, and size might significantly change from that initially developed because of dissolution and agglomeration.[6,7] Furthermore, there have been concerns raised as to the cleanliness and corrosion resistance of carbon support materials in fuel cells, especially because they are exposed to the reaction environment to a great extent. The stability of the catalyst support against corrosion at high electrode potentials experienced as a result of fuel starvation from water blockage, stop−start, and other real dynamic phenomena is a critical durability issue.[8–11]

Long-term durability and high performance are expected to be achieved with low precious metal content, that is, using low metal loadings on a support material. In fuel cells for automotive applications, it has been suggested that the total Pt loading should be decreased by ~4-fold from that level currently used, down to 0.20 mg_{Pt} cm^{-2}, while at least the same activity should be maintained.[7] Given the sluggish kinetics of the cathodic oxygen reduction reaction (ORR), meeting such targets requires significant improvements in Pt mass-specific surface area [m^2_{Pt} g_{Pt}^{-1}] and Pt surface area-specific activity [A cm^{-2}_{Pt}].

The use of the crystallized form of an organic pigment, *N*,*N*-di(3,5-xylyl)perylene-3,4:9,10bis(dicarboximide), referred hereafter as perylene red (PR149), as the PEM fuel cell electrocatalyst support was introduced by Debe et al.,[12–14] and such an electrocatalyst system is referred to as the nanostructured thin-film (NSTF) catalyst.[13] The unique fabrication process and growth mechanism for generating this nanostructured thin-film support structure were described in detail earlier by Debe and Poirier of the 3M Company.[14] They reported that vacuum-annealing converts the initial as-deposited smooth organic film to an extremely dense and "randomlike" array of discrete whiskers with areal number densities controlable in the range from 3 to about 10 billion cm^{-2}, that are uniformly oriented with their long axes normal to the substrate. The whiskers are crystalline, and subsequently have been shown to have high thermal, chemical, and electrochemical stability under the operation conditions relevant to PEM fuel cells.[13,15] Structural characteristics of the PR149 support whiskers as determined by electron diffraction are presented elsewhere.[12] In brief, the whiskers' morphology comprises rectilinear lath-shaped crystalline elements with controllable lengths in the range from about 300 to over 1500 nm depending on the thickness of the starting film used to grow them. The whiskers have mean cross-sectional dimensions of 52.5 ± 12.0 and 27.0 ± 7.5 nm that are determined by the ratio of surface free energies of the whisker side-planes and, therefore, are less controllable by the process used to grow them. Such structural dimensions imply surface area enhancements by a factor of 5–15, depending on the areal number density and length of the whiskers.

In the NSTF electrocatalysts, another level of surface roughness is introduced when the layer of oriented mesostructured perylene red whiskers is conformally coated by a metal film, that is, when the support organic whiskers are covered by a catalyst (i.e., platinized). The vacuum-deposition method, process conditions, and materials can all influence the roughness of the catalyst coating on the whiskers. Conventional electron microscopy imaging for the individual whiskers has shown already[13] that under some deposition conditions, the catalyst coating comprises a monolayer of closely packed but seemingly separated acicular-shaped metal grains (referred to as whiskerettes) that are uniformly oriented, off-normal to the side planes of the crystalline PR149 whisker. The individual nanoscopic metal whiskerettes are found to be highly crystalline.[13] It should be noted that this is a unique physical characteristic in contrast to the largely amorphous metal structures formed by their deposition onto carbon black by dual-ion beam-assisted deposition (IBAD).[16] It has been shown that the PR149 support whisker's surface area, as well as the metal loading, affects the metal grain size,[13] as in case of Pt dispersed on carbon-supported electrocatalyst systems (Pt/C). The coverage by the metal on the two supports however is quite different. First of all, except for ultra low loadings (for Pt on appropriately sized whiskers, this means below 20 μg of Pt per cm^2), all of the PR149 surface area is coated, and the support material is encapsulated by a thin polycrystalline metal layer. Furthermore, while an increase in the weight percent Pt/C loading results in an increase in size or in areal number density of carbon-supported nanoparticles,

(3) Haruta, M.; Tsubota, S. In *Catalysis and Electrocatalysis at Nanoparticle Surfaces*; Wieckowski, A., Savinova, E., Vayenas, C., Eds.; Decker: New York, 2003; p 645.
(4) Coq, B.; Figueras, F. In *Catalysis and Electrocatalysis at Nanoparticle Surfaces*; Wieckowski, A., Savinova, E., Vayenas, C., Eds.; Decker, New York, 2003; p 847.
(5) Burda, C.; Chen, X.; Narayanan, R.; El-Sayed, M. A. *Chem. Rev.* **2005**, *105*, 1025.
(6) Horky, A. In *Fuel Cells Durability—Stationary, Automotive, Portable*, 1st ed.; Knowledge Press: Brookline, MA, 2006; p 133.
(7) Gasteiger, H. A.; Kocha, S. S.; Sompalli, B.; Wagner, F. T. *Appl. Catal., B: Environ.* **2005**, *56*, 9.
(8) Tang, H.; Qi, Z.; Ramani, M.; Elter, J. F. *J. Power Sources* **2006**, *158*, 1306.
(9) Roen, L. M.; Paik, C. H.; Jarvi, T. D. *Electrochem. Solid-State Letters* **2004**, *7*, A19.
(10) Ferreira, P. J.; la, O. G. J.; Shao-Horn, Y.; Morgan, D.; Makharia, R.; Kocha, S.; Gasteiger, H. A. *J. Electrochem. Soc.* **2005**, *152*, A2256.
(11) Li, W. In *Fuel Cells Durability—Stationary, Automotive, Portable*, 1st ed.; Knowledge Press: Brookline, MA, 2006; p 101.
(12) Debe, M. K.; Drube, A. R. *J. Vac. Sci. Technol., B* **1995**, *13*, 1236.
(13) Debe, M. K. In *Handbook of Fuel Cells—Fundamentals, Technology and Applications*; Vielstich, W., Lamm, A., Gasteiger, H. A., Eds.; Wiley: New York, 2003; Vol. 3, Chapter 45.
(14) Debe, M. K.; Poirier, R. J. *J. Vac. Sci. Technol.* **1994**, *12*, 2017.
(15) Debe, M. K.; Schmoeckel, A. K.; Vernstrom, G. D.; Atanasoski, R. *J. Power Sources* **2006**, *161*, 1002.
(16) Saha, M. S.; Gulla, A. F.; Allen, R. J.; Mukerjee, S. *Electrochim. Acta* **2006**, *51*, 4680.

the increase in Pt loading in the NSTF systems is manifested as an elongation of the PR149 whisker-supported metal whiskerettes. The dimensional aspect ratio of the whiskerettes varies along the long axis of the whisker particle. For example, for the PtRu NSTF sample discussed in ref 13, the whiskerettes feature ~8 nm diameter cross-sectional dimensions and varying length up to 30 nm, depending on the position along the whisker's length. In general, the roughness of the metal coating on the sides of the whiskers can vary from very smooth to very rough. However, even when the catalyst coating on a single whisker particle exhibits a large roughness factor, the measured electrochemical surface area for NSTF-Pt is many times less than that for conventional Pt/C layers of the same loading.[13] At the same time, the Pt surface area-specific oxygen reduction activity of the NSTF catalyst systems are found to be ~10 times higher than that obtained for high surface area Pt/C electrocatalysts.[30,31] As a result, similar Pt mass-specific activities are obtained with NSTF Pt alloys as with the state-of-the-art PtCo/carbon electrocatalysts.[32]

The source of the activity gain with NSTF electrocatalysts is not completely understood. As proposed by Debe,[13] it might have contributions from the nature of metal/support interactions, the enhanced ionic transport at the interface of the catalyst surface and the membrane, or the differences in the type and degree of metal faceting, lattice strain, or surface defects. Variations in surface morphology are considered as the primary origin of the so-called crystallite size effects in electrocatalysis.[17] Faceting or the formation of surface defects are known to have a large influence on ORR,[17,18] as well as on the electrooxidation of chemisorbed carbon monoxide,[18–20] and hence can alter electrocatalysis in hydrogen fuel cells on both the cathode and anode sides, respectively. It is important to note that the Pt surface-area-specific ORR activity with pure Pt NSTF matches those obtained with bulk polycrystalline Pt electrodes as determined using rotating ring disk electrode experiments.[30,31] This suggests the largely continuous nature of the thin film catalyst encapsulating each PR149 whisker particle is an important attribute leading to high surface area-specific activity, similar to the way in which the extended two-dimensional nature of the bulk polycrystalline Pt is a key property for achieving high Pt surface area-specific activity.

While the mesoscopic physical and chemical characteristics of the PR149 material were previously discussed in great detail,[12–14] only a limited amount of work has concerned the morphology of the deposited metal (alloy) films. A preliminary EC-IRAS study has shown that the PR149-supported Pt NSTF exhibits voltammetric and surface vibrational properties similar to those of polycrystalline Pt.[21] The predominance of surface (111) facets was also suggested on the basis of the preliminary data obtained by high resolution transmission microscopy (HRTEM) imaging.[21] The Berkeley group approximated the NSTF-Pt simply as a 30 nm particle electrocatalyst system with a large number of defect sites and irregularities to compare its electrochemical properties to conventional carbon-supported samples.[19,20] They also interpreted CO electrooxidation and ORR activity data by making that approximation.[17]

In this paper, the equilibrium crystallographic characteristics of the crystalline whisker-supported Pt-based NSTF electrocatalysts are presented based on atomic-resolution electron microscopy images (via HRTEM) and surface energy considerations.[22] Fundamentals of the atomic-resolution real space HRTEM imaging, the image interpretation, and methodology for resolving structure of nanocrystals are available elsewhere.[26,27] We propose a model for metal crystal growth on the PR149 whisker support that explains the observed trends in equilibrium shapes and faceting.

II. Experimental Section

1. Preparation of the Nanostructured Thin-Film Electrocatalysts. The NSTF electrocatalysts were prepared at 3M Company as described elsewhere.[12–14] In brief, the organic support consists of a monolayer of oriented crystalline whiskers of an organic pigment material, *N*,*N*-di(3,5-xylyl)perylene-3,4:9,10bis(dicarboximide), (referred to hereafter as PR149). The NSTF catalyst-coated whiskers are formed in a web-coating process as a roll-good on a microstructured catalyst transfer substrate (MCTS).[13] The metals are sputter-coated on top of the PR149 whiskers so as to encapsulate each support whisker with a polycrystalline thin metallic film. The composition and structure of the metal coating were adjusted by the power levels and compositions of the sputtering targets. The loading of the pure Pt samples was adjusted in between 0.15–0.22 mg_{Pt} cm^{-2}. The PtRu binary alloy NSTF samples were prepared using two separate targets, pure Pt and pure Ru, to give a Pt loading of 0.22 mg cm^{-2} Pt and a Pt/Ru atomic ratio of ~1. The Pt-based ternary alloy NSTF was made using a Pt and a NiFe target consisting of Ni and Fe at the atomic ratio of 90:10. The total Pt loading of the PtNiFe NSTF was 0.1 mg cm^{-2}. The ratio of Pt to Ni + Fe was determined by controlling the relative thickness of the deposited layers. The total number of layers was determined by the desired loading of Pt. The NSTF whiskers are then transferred to the surface of a proton exchange membrane using a hot-roll lamination process to form a catalyst-coated membrane for use in a fuel-cell membrane electrode assembly (3M-cast Nafion, 1000 EW, 30 μm thick). The catalyst coated whiskers were removed from the MCTS surface by brushing to obtain powders to form aqueous suspensions for TEM characterization.

2. Transmission Electron Microscopy. Conventional bright field (BF) and dark field (DF) TEM images were obtained using a JEOL 2010 LaB6 microscope. High-resolution transmission electron microscopy (HRTEM) and scanning transmission electron microscopy (STEM) measurements were carried out using a JEOL 2010F analytical electron microscope (AEM). The AEM was equipped with a Schottky field emission electron gun operating at 200 kV. The microscopes are computer-controlled through the JEOL FasTEM interface system. Micrographs were recorded digitally by

(17) Mayrhofer, K. J. J.; Blizanac, B. B.; Arenz, M.; Stamenkovic, V. R.; Ross, P. N.; Markovic, N. M. *J. Phys. Chem. B* **2005**, *109*, 14433.
(18) Markovic, N. M.; Ross, P. N. *Surf. Sci. Rep.* **2002**, *45*, 117.
(19) Arenz, M.; Mayrhofer, K. J. J.; Stamenkovic, V.; Blizanac, B. B.; Tomoyuki, T.; Ross, P. N.; Markovic, N. M. *J. Am. Chem. Soc.* **2005**, *127*, 6819.
(20) Mayrhofer, K. J. J.; Arenz, M.; Blizanac, B. B.; Stamenkovic, V.; Ross, P. N.; Markovic, N. M. *Electrochim. Acta* **2005**, *50*, 5144.
(21) Wieckowski, A.; Gancs, L.; McGovern, M.; Lu, G.-Q.; Atanasoski, R.; Debe, M. K. Presented at the 227th ACS Meeting, Anaheim, CA, March, 2004, Abstract COLL-260.
(22) Markovic, N. M.; Radmilovic, V.; Ross, P. N., Jr. In *Catalysis and Electrocatalysis at Nanoparticle Surfaces*; Wieckowski, A.; Savinova, E.; Vayenas, C.; Eds.; Decker, New York, 2003; p 311.
(23) Wang, Z. L. *J.Phys. Chem. B* **2000**, *104*, 1153.

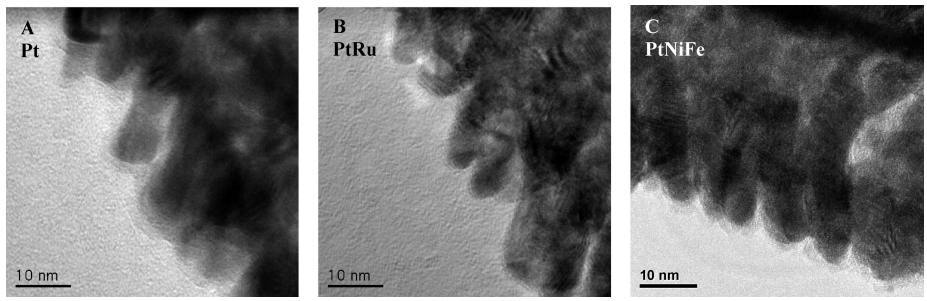

Figure 1. HRTEM images of typical (A) Pt, (B) PtRu, and (C) PtNiFe metal crystallites supported on PR149 organic whisker particles. The magnification is 600 000.

a slow-scan charge-coupled device (CCD) and were processed using the DigitalMicrograph 3.6.5. software (Gatan Inc., U.S.A.). An ~10 μL drop of a water-based suspension of the NSTF catalyst coated whiskers was deposited onto a carbon film-coated copper mesh. The porous carbon grid specimen was then dried under a heat lamp at moderately high temperature and examined ex situ in a double-tilt TEM holder.

III. Results and Discussion

1. General Structural Characteristics. Physical and chemical properties of the PR149 organic pigment support have been discussed in great detail previously based on conventional TEM imaging and electron diffraction data.[12–14] The PR149 support layer is composed of a densely packed array of rectangular lath-shaped crystalline whiskerlike particles, which have side dimensions in the range of a few tens of nanometers and, for the samples used in this study, lengths on the order of 1 μm. In addition to the ~5−10-fold increase in roughness factor that the monolayer of whiskers enables, the fine structure of the metal film deposited onto the whiskers adds another level of surface roughness with respect to the geometric surface area. In the work reported here, the sputtered Pt and Pt alloy metals are found to form as distinct nanosized crystallites, referred to as whiskerettes,[13] on the side planes of the PR149 whisker particles. The metal whiskerettes exhibit size dimensions in the range of a few nanometers with dimensional aspect ratios in the range of 1−5. Such a morphology of the NSTFs yields surface areas multiple times higher than a smooth metal coating would provide on other support materials. To reveal the structural characteristics of the catalytic metal whiskerettes and also to find the reasons behind their growth habit, Pt, PtRu, and PtNiFe NSTF catalyst systems were subjected to a comprehensive analytical electron microscopy study. It was previously shown, using electron diffraction,[14] that the crystalline whisker has a body centered cubic (bcc) lattice structure, with [111] side facets, [01$\underline{1}$] edge facets, and a [211] growth tip. The bcc lattice constant is 14.5(4) Å, and four PR149 molecules constitute a conventional unit cell (two molecules per each primitive lattice point).[14] Extensive XRD analyses of the Pt and Pt-alloys suggested[24,25] that the NSTF electrocatalysts are substitutional alloys having face centered cubic (fcc) structures, as should all of those studied in this work. Figure 1A−C manifests that all three metal whiskerette types (Pt, PtRu, PtNiFe) display very similar morphological characteristics to one another. As the micrographs demonstrate, the metal cluster morphology is indeed unique and quite different from those of any conventional nanoparticle catalyst. In the following, we will discuss the general structural characteristics of the PtNiFe ternary NSTF catalysts with various electron microscopy imaging strategies.

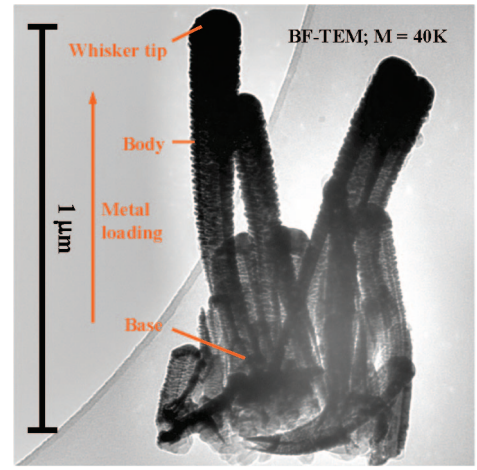

Figure 2. BF-TEM image for a cluster of PR149 whisker particles carrying a typical Pt loading.

2. Catalyst Coating Morphology. Distribution of the metal coating on the PR149 whisker particle was analyzed on the bright field (BF) images. Figure 2 shows a BF TEM image of a cluster of the catalyst-coated, PR-149 whisker particles. Since growth of the PR149 whiskers follows a screw dislocation growth mechanism,[14] the length of the whisker particles and, to some extent, their areal number density can be controlled during sample preparation. The typical length of the whisker particles for all samples used in this study is ~0.8 μm. For the PtNiFe alloy at relatively heavy loading of 0.2 $mg_{Pt}\ cm^{-2}$, the alloy coverage is clearly not uniform along the longest axis of the lath or columnar-shaped support whiskers. Such a loading profile is caused by self-shadowing effects during sputter deposition of the metal onto the densely packed whisker columns. The extent of the nonuniformity depends on the whisker length and spacing, as well as on the metal loading. For a typical whisker

(24) Bonakdarpour, A.; Lobel, R.; Atanasoski, R. T.; Vernstrom, G. D.; Schmoeckel, A. K.; Debe, M. K.; Dahn, J. R. *J. Electrochem. Soc.* **2006**, *153*, A1835.

(25) Bonakdarpour, A.; Wenzel, J.; Stevens, D. A.; Sheng, S.; Monchesky, T. L.; Lobel, R.; Atanasoski, R. T.; Schmoeckel, A. K.; Vernstrom, G. D.; Debe, M. K.; Dahn, J. R. *J. Electrochem. Soc.* **2005**, *152*, A61.

(26) Williams, D. B.; Carter, C. B. *Transmission Electron Microscopy: A Textbook for Materials Science*; Plenum Press: New York, 1996.

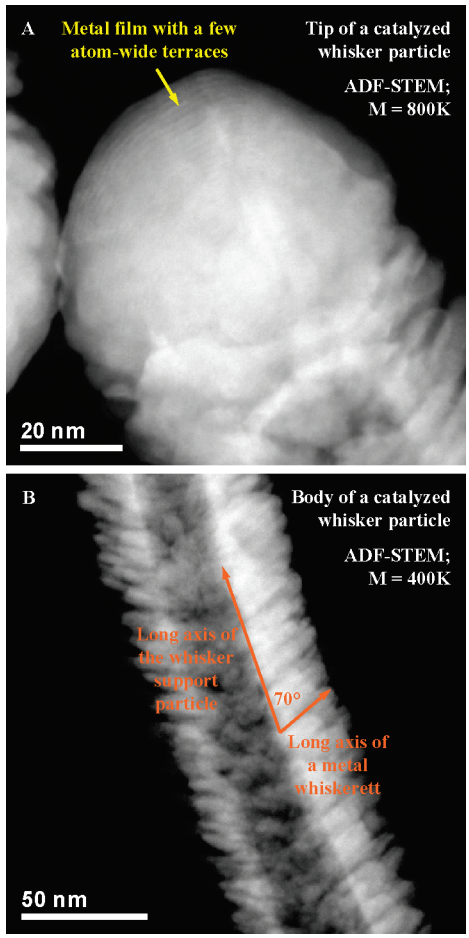

Figure 3. ADF-STEM images for the (A) "tip" and (B) "body" of a PtNiFe alloy-coated PR149 whisker particle.

particle studied for pure Pt loading (on the order of 0.1 mg_{Pt} cm^{-2}), the metal distribution is quite uniform but is rather uneven at the higher loadings used for the PtNiFe system studied in this work.

Metal dispersion on a single PR149 support particle can be viewed by selection of an individual whisker (Figure 3). Since the whiskers are distributed quite uniformly and are oriented with their long axes generally perpendicular to the substrate's surface, a heavily loaded whisker tip develops during metal coating, which generally faces the direction of the deposition. (There is not a fixed angle of deposition of the metals relative to the PR149 crystalline whiskers for two reasons. First, the whiskers are grown onto substrates that are roll-good webs of polyimide having a microstructured surface consisting of V-shaped grooves 6 μm tall and 12 μm peak-to-peak. The whiskers tend to grow perpendicular to their local substrate and hence point in generally orthogonal directions on alternate sides of each substrate V-groove. The V-grooves are parallel to the down-web direction. Second, the catalyst was sputter-deposited onto the whisker coated substrate as the web passed underneath planar magnetron targets, causing the line-of-sight angle of incidence to vary significantly over the time of passage under the targets.) It may also be important that the tip of the crystalline whisker is the site of a screw dislocation[14] because this could contribute to the very different Pt film structure seen on the whisker tips compared to the whisker sides. Below the tip, the metal coverage progressively decreases toward the whisker base down to where the whisker is attached to the MCTS substrate. While keeping the amount of the deposited metal the same, the dispersion can be increased by increasing the length of the PR149 support particles.

The equilibrium morphological characteristics of the metal coating on the PR149 support are discussed based on the annular dark field (ADF) scanning transmission electron microscopy (STEM) images presented in Figure 3. The images display strong mass-thickness contrast and thereby provide another picture of the metal dispersion on the organic whisker support particle. Basically, the deposited metals are incorporated into three main differently structured domains on the PR149 whiskers. The metal atoms become incorporated into the whisker tip (Figure 3A) or form whiskerettes of similar shape but of varying lengths along the long axis of the whisker particle (Figure 3B), or where the metal loading is low at the base of the whiskers, it appears to form a finely grained film (low aspect ratio whiskerettes) (not shown in Figure 3B). No other types of metal structures were observed in the metal coatings encapsulating any whisker. The surfaces of the metal-covered whisker tips consist of small terraces that are evenly separated by steps of a few nanometers. This is apparent in Figure 3A, where the dense and parallel lines on the tip of the whisker represent the edges of those terraces. Nevertheless, the surface structure of the tip is much smoother compared to the rough whiskerette metal coatings seen in the other two coating domains on the whisker support. Although the tip of the rectangular prism-shaped PR149 whisker holds the highest metal mass per unit support surface area, only a fraction of the total mass of the deposited metal accumulates therein. Also, the tip is found to be the only part of the whisker particle where the metal crystallites are agglomerated (Figure 3), which also reduces the surface area per unit mass of metal accumulated there. Hence, the majority of the metallic surface area of the metal on any given whisker is determined by the surface area (dimensions) of the metal whiskerettes and their areal number density on the sides of a whisker (Figure 3B).

We next focus on the nanoscale morphology, as well as on the dimensions and faceting of the metal whiskerettes. Even though the deposited metal film can encapsulate a PR149 support particle, as indicated above, it does not appear to be fully continuous in the vicinity of the whisker particle's base. Here, the population density, shape, and dimensions of the metal whiskerettes are markedly different from those located on parts higher up the whisker particle. The HRTEM image in Figure 4A taken of the base of a whisker particle shows the smallest metal crystallites that can be found in these examples. An extensive HRTEM study of such domains provided insights into the nucleation and growth mechanism of the metal whiskerettes on the PR149 whisker support particles. For instance, particularly low electron yields could be detected through the edges of the PR149 whisker particle, suggesting that the preferred surface sites to anchor metal atoms are located on the bcc [211] edges of the lath-shaped whisker crystals. In fact, TEM images of the small metal clusters nucleated along step edges (located

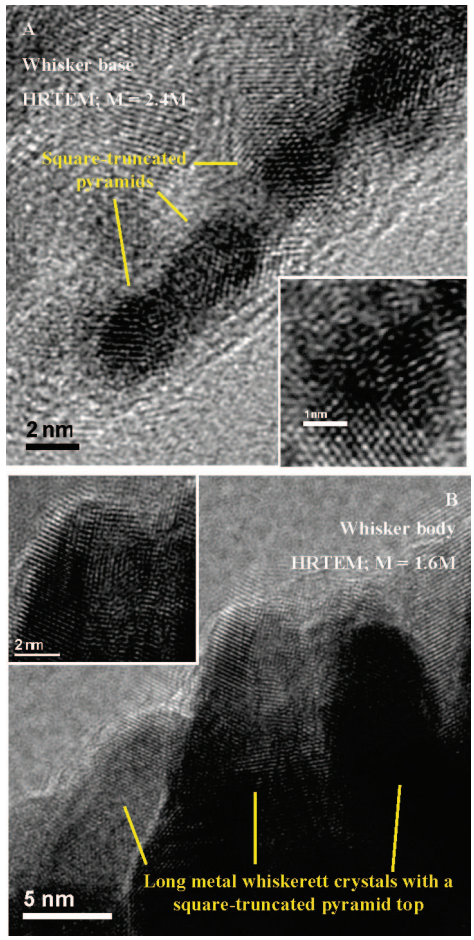

Figure 4. HRTEM images for PtNiFe alloy crystallites located (A) at the "base", and (B) on the "body" of a PR149 whisker particle. The insets zoom onto selected crystallites having typical morphology.

parallel to the whisker long axis) provided the first evidence of the crystalline nature of the PR149 whisker supported element.[12] Also (not shown) metal crystallites nucleate on the wider [111] side planes of the whisker body as well, apparently associated with defects.[12] In general, in the present TEM study, the whiskerettes are observed to nucleate and grow on particular surface sites that are evenly separated from each other by ~6–8 nm. Under moderate and high metal loadings, a PR149 whisker surface becomes fully covered by the metal whiskerettes as their bases fuse together. However, the bodies of the whiskerettes remain distinct from their nearest neighbors, and project off the long axis of the rectangular lath-shaped whisker at an identical angle of 70 ± 1° (Figure 3B). Note that the angle is the same as the angle between the (111) crystal planes in cubic lattices, namely, 70.53°. The alignment of the whiskerettes indicates the preferred direction of metal crystal growth thereby giving us a preliminary idea about the preferential surface faceting of the metal layers at the interface with the PR149 crystalline support whisker. Given the range of incidence angles seen during catalyst deposition, both spatially and temporally as described above, but the existence of just one common and highly consistent orientation angle of 70° between the whiskerette axes and the axis of the whisker they coat, suggests that the interaction of the deposited atoms with the whisker's crystalline sides, that is, a substrate driven growth mechanism, is determining the whiskerettes' orientation angle rather than deposition process factors such as angle of incidence.

Another commonly unique structural characteristic of the PR149-supported samples concerns the topography of catalyst crystallites on the support particle. Figures 1, 2, 3B, and 4A demonstrate the highly ordered layout of whiskeretts on a whisker particle. The whiskeretts are separated evenly by ~6–8 nm, although they seem to nucleate preferentially along the edges. In contrast, a great wealth of available electron microscopy data attests that the arrangement of nanoparticles on conventional carbon flakes is irregular. On a typical carbon flake, surface electron density is expected to vary randomly according to the amorphous nature of the particles at and above the nanoscale level. Catalyst nanoparticles tend to nucleate at those random surface irregularities, as well as at the edges of fine pores described with high reactivity. This trend is manifested by the effective clogging of small pores on a carbon flake by the catalyst nanoparticles. For evidence, the BET mass-specific surface area for Vulcan XC72-R carbon black drops dramatically, from 281 to 178 $m^2\ g^{-1}$, when even just 10 wt % Pt is dispersed on it. (The BET surface area of the unsupported Pt catalyst crystallites is negligible compared to that of the carbon material.) At the same time, the nucleation pattern of catalyst whiskerette crystallites on a whisker support appears to follow regular fluctuations in surface electron density that are likely determined by some periodic macromolecular characteristics of the PR149 particle surface. In summary, such nucleation preferences and the unique shape, growth mechanism, and uniform alignment of catalyst whiskerette crystallites in the NSTF samples all point to the instrumental role of the PR149 support material in the development of surface, and ultimately, electrocatalytic properties. The growth mechanism as well as the structural properties of the catalyst crystallites is discussed in detail in the following sections.

The influential role of the PR149 support-metal interactions in developing the unique nanoscale morphological features of the NSTF catalysts is manifested by the morphology and the size distributions of the whiskerettes on a selected whisker particle. As seen in Figure 1 and 3B, the great majority of the metal crystallites have a similar shape and well-defined geometry, which is the representative form at the moderately and heavily loaded parts of the PR149 whisker. This observation is further supported using HRTEM in which phase modulation of the incident electron wave is the dominating imaging mechanism (resulting in a fine contrast in the atomic distribution function). In other words, the high resolution electron micrographs can be analyzed and discussed also as thickness-projected images of the crystallites. In addition to the phase contrast, the diffraction (or amplitude) contrast contributes to the development of the HRTEM images. This contrast mechanism helps us to reveal the borders of the crystallites as well as the edges of the surface planes. By taking images of a selected metal crystallite at various orientations, the 3D geometry of the whiskerettes could be resolved.[23] Figure 4 presents two characteristic whiskerette shapes, which could be found on a whisker particle. For the smallest metal crystallites, which

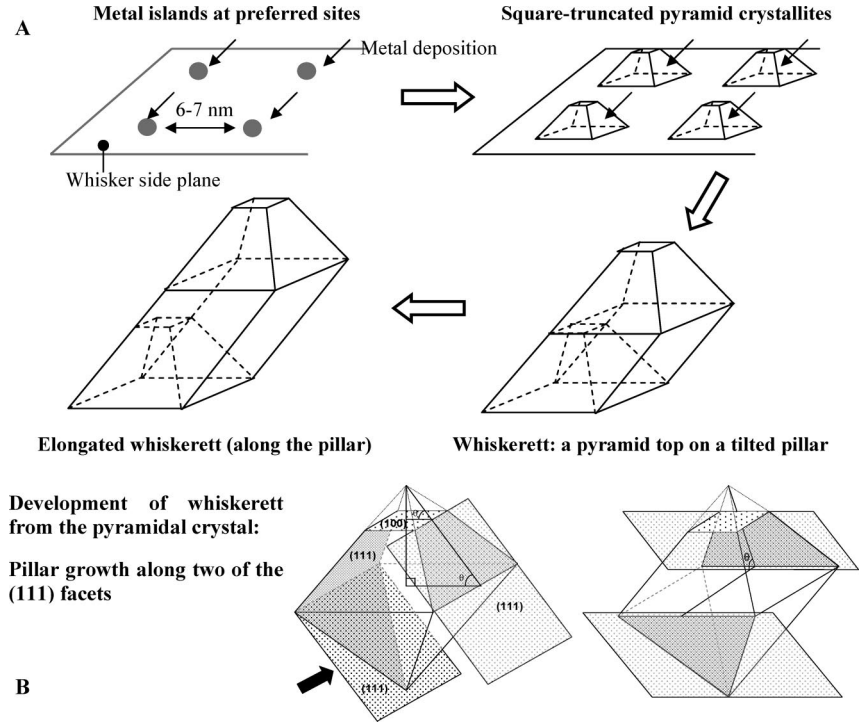

Figure 5. Schematic illustration of the growth mechanism of metal crystallites in the PR149-supported NSTF electrocatalysts. Panel A displays the typical metal structures at various stages of the crystallite growth process, and panel B demonstrates the development of whiskerette pillars in terms of surface faceting.

are located at the base of the whisker particle (where the metal loading is low) the equilibrium morphology can be described using the square-truncated pyramid geometry. Such crystallites are pictured in Figure 4A. In the inset, one selected metal particle is shown at higher resolution to facilitate resolving the geometry. The majority of the metal crystallites appear as acicular whiskerettes, which look like elongated columns with the square-truncated pyramids preserved on top. Figure 4B and the inset therein provide evidence for such geometric structure of the typical whiskerettes that form the PR149-supported NSTF electrocatalysts.

3. Proposed Mechanisms for Whiskerette Crystal Growth and Equilibrium Surface Faceting. As discussed in the previous section, the sputtered metals develop into highly uniform crystalline whiskerettes rather than forming largely amorphous layers (like those on conventional carbon support materials). To explore their unique surface characteristics, which we propose originate from the molecular structure of the organic whisker support material, a pragmatic HRTEM imaging tactic was employed. Namely, the evolution of the whiskerette's equilibrium geometric shapes (Figure 4) can be understood by imaging and resolving the morphology and surface structure of the metal crystallites as they develop along the longest axis of a PR149 whisker particle. Again, a typical whisker support particle demonstrates an increase in the metal loading from its base to its tip. In large part, this is caused by self-shadowing effects causing the rate of deposition to be lower at the base of the oriented whiskers than at the top. The analysis of the variations in the number density, shape, and dimensions of the metal whiskerettes along the long axis of a whisker particle gives us some information on the crystal growth mechanism. A simple model can be set up for the growth mechanism of metal crystallites on the NSTF PR149 whisker support (see below).

The proposed whiskerette growth model is illustrated in Figure 5. As shown on the micrograph taken of the base of the PR149 whisker particle (also in Figure 4A), the deposited metal atoms first take up some preferred sites on the support material and arrange into small patches (islands). This tendency can clearly be seen in Figure 1 of ref 12, where 2 nm clusters clearly decorate the linear step edges of the whisker's crystalline side planes. On the lightly metal-loaded parts, where the early stage of crystal growth can be examined, small pyramids develop. The peak of the pyramids was found to be truncated by a flat square. Such pyramids are imaged in Figure 4A. The square-truncated pyramids' edge lengths have small dimensions, less than 8 and 3 nm for the base and the square-top edges, respectively. In the truncated pyramid crystallites, the aspect ratio of the base to the top-square edge lengths is found to be ~8:3.

The truncated pyramid geometry can be anticipated by considering surface free energy for platinum-based crystallites. Simply put, the facets tend to be formed by truncating a crystal in such a way that it will increase the proportion of the low Miller index planes. Generally, the following sequence is held for the magnitude of surface free energy of the basic crystallographic planes: (111) < (100) < (110).[23] It may therefore be expected that the small fcc crystallites will expose predominantly the (111) facets. From the spatial domain images of the metal crystallites, diffractograms were generated via fast Fourier transformation (FFT). By indexing the diffractograms based on the measured lengths of the two vectors and the contact angle in between them,[26] the surface faceting of the truncated pyramids could be revealed. In

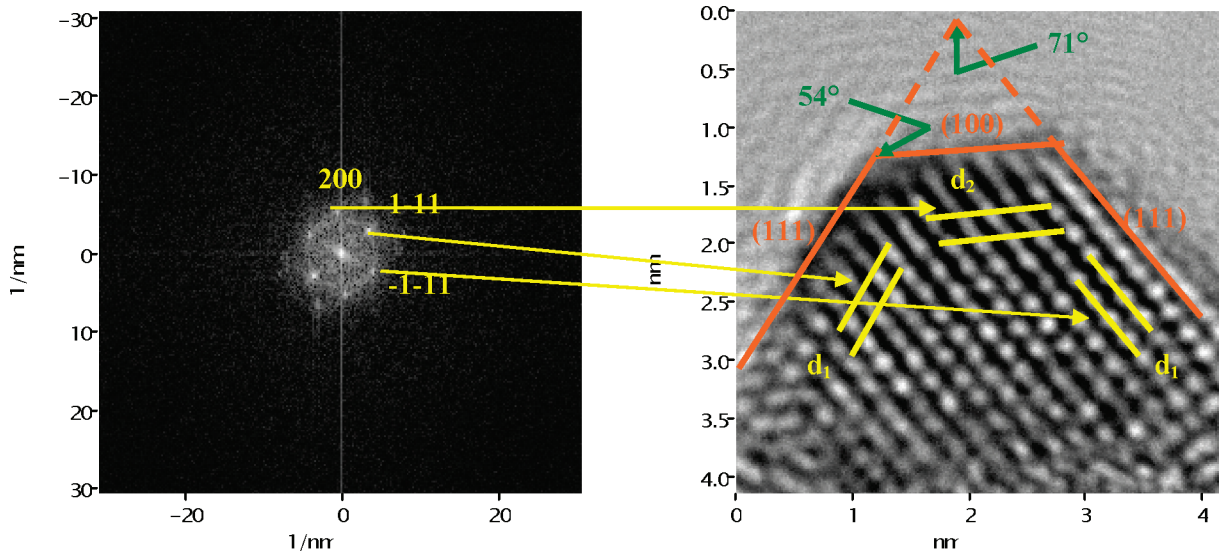

Figure 6. Indexed diffractogram of a typical pyramid-shaped tip of a PtNiFe whiskerette particle and the corresponding crystal planes and lattice parameters as shown on the reciprocal space image.

Figure 6, a diffractogram is shown for a square-truncated pyramid metal crystallite facing the incident beam direction of [100]. The pattern indices were obtained based on the data in ref 26 and were then correlated to the crystal planes after converting the diffractogram back to the spatial domain image using inverse FFT. As expected from surface energy minimalization, the smallest metal crystallites ideally expose four large (111) and one small (100) single crystal facets. On the basis of the geometric model, the edge and corner atoms make up less than 15% of the total number of surface atoms for the crystallites larger than a few nanometers. For the majority of the whiskerettes, the number of corner and edge atoms is negligibly small. Consequently, adsorption properties of the (111) single crystal planes in the NSTF electrocatalysts should play a dominant role in ORR reactions. As mentioned above, the small pyramids expose a (100) facet, which truncates the pyramid peak.

To further rationalize this faceting behavior, we calculated the geometric surface area as well as the surface free energy at various ratios ($r = l_{top}/l_{base}$) of the truncated pyramid's top and base facet side lengths. When r approaches zero, the equilibrium shape approaches a perfect rather than a truncated pyramid. Data for the square-truncated pyramid of a 50 nm^3 volume, roughly representative of the small crystallites (see HRTEM images), are obtained by application of the embedded-atom-function calculation and using the parameters reported in ref 27. Figure 7 summarizes the results. The plots indicate that the surface area as well as the surface free energy is minimal when r is approximately 0.3. In other words, the surface free energy of a (100) plane-truncated pyramid crystallite is lower than that of a perfect pyramid for the same crystal volume. The calculated optimal value of 0.3 for r is in fact in a good agreement with the observed value of $r \approx 3/8$ discussed above.

On the more typical acicular-shaped whiskerettes, formed higher up the whisker toward its tip (Figure 4B), the truncated pyramid shape is still preserved and constitutes the top portion of the whiskerette. Such long metal whiskerette

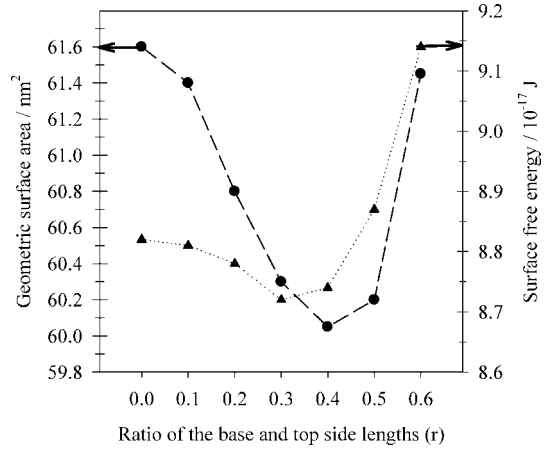

Figure 7. Plot of the geometric surface area, as well as the surface free energy, as a function of the ratio of the lengths of top and base side edges for a 50 nm^2 square-truncated pyramid metal crystallite.

crystallites cannot be described by the truncated pyramid geometry but appear much elongated. As depicted in Figure 5A, the growth of whiskerettes takes place by keeping the initial pyramidal structure, while the metal crystallites grow further in one direction while developing into a long pillar. Again, the truncation of the whiskerette tip results from the tendency to reduce the surface energy. This also applies to the mechanism of the pillar growth as illustrated in Figure 5B. The growth and elongation of the pillar can readily be understood based on the surface free energy order of the low index crystal planes.[23] As demonstrated in Figure 5B, the pyramid, which is considered as the elementary shape of a cuboctahedron, grows so as to extend two of its (111) facets. The elongated pillars exhibit gradually increasing length toward the whisker particle top. This results in a progressively higher metal loading toward the whisker tip. Interestingly, the pillars do not fuse together with each other while growing, but remain as distinct metal crystallites, featuring small dimensions along their short axes. While the whiskerette length may increase up to 25 nm, its width does not significantly deviate from ~6–7 nm, which is consistent

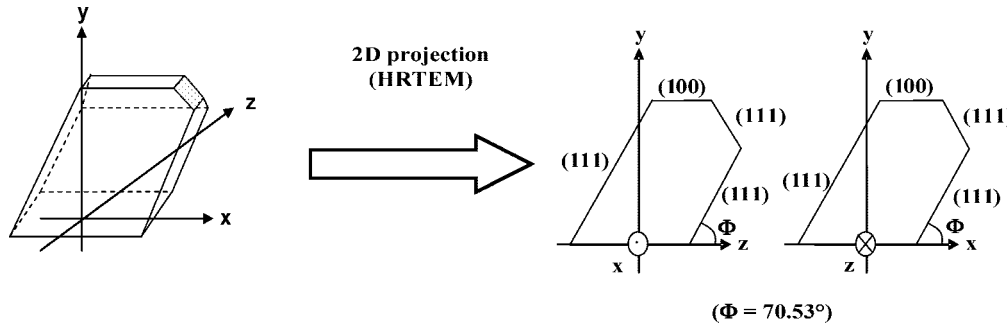

Figure 8. Three dimensional sketch for a typical whiskerette particle that is tilted by 70.5° with respect to the whisker substrate's [111] plane and the two-dimensional projections.

with the maximum edge length of the pyramid's square base. The fact that the whiskerette cross-sectional dimensions do not change as their length changes is consistent with Wulff's theorem[33,34] for submicron sized crystals, the same reason the cross-sectional dimensions of the larger PR149 whiskers do not change as they grow longer, namely, the surface free energy per unit area of crystal face (*hkl*) is proportional to the distance of the crystal face from the center of the crystal.

Another remarkable characteristic of the whiskerette growth is that the whiskerettes become aligned so that they project off the side planes of the whiskers in a uniform direction tilting toward the whisker top. The whiskerette long axes and the whisker long axis display a uniform angle of ~70°. We surmise this orientational angle results from the influence of the bcc (111) surface of the wider sides of the crystalline PR149 whiskers,[12] resulting in an "epitaxial-like" Pt(111) nanoisland growth of the first few monolayers on the PR149(111) surface.

The question of why the whiskerettes are uniformly oriented in one direction, pointing toward the tips of the whiskers rather than their bases or any of four other possible directions for (111) symmetry, is of interest. This preference for one of the six possible directions is probably a result of the fact that the direction of the incidence of the incoming metal atoms is predominantly from the top of the whiskers during the sputter deposition process.

On the basis of the above proposed growth model, the structure of a typical whiskerette was constructed and is outlined in Figure 8. By showing the two-dimension projections, the analogy to the HRTEM micrographs (Figure 3B) is apparent. Figure 8 demonstrates a tilted alignment of the whiskerettes with respect to the side plane of the whisker support particle, as it is confirmed in the HRTEM micrographs (Figures 1 and 3B). It is furthermore expected that the whiskerettes will show predominantly the (111) surface sites, although the ratio of the (111) to the (100) or other low-coordination (edge, vertex) sites should decrease as the metal loading decreases. This will cause the lengths of the whiskerette pillars to decrease. Given different ORR activities of the different Pt(hkl) facets,[18] this effect might imply that the effective specific activity would also decrease with loading since the proportion of the surface area of the most active Pt(111) facets would decrease.

4. Surface Properties and Implications for Activity. Although the elemental composition of the catalyst surface is of crucial importance in electrocatalysis of typical fuel cell reactions, surface morphology also plays a significant role in product distribution and rate of such reactions.[18] This is rationalized by examining the adsorption geometry and the reaction heat of adsorption involved in the reactions.[17,28,18,20]

As demonstrated above, surface properties of the PR149 crystalline whisker-supported NSTF catalysts are unique and can be tailored by the deposition practice. The Wulff construction of the whiskerettes[29] reveals that the typical PR149-supported metal crystallites expose six (111) and only one (100) plane. We have shown that a typical whiskerette exposes predominantly the (111) terrace sites and only a few (100) terrace sites (see Figures 5B, 6, and 8). Again, the long pillar base is bound by the (111) planes and the surface area of those planes provides the majority of the total metallic surface area at a typical metal loading. Essentially, the PR149-supported NSTF electrocatalysts can be considered as (111) single crystals with some surface defects. Nevertheless, the proportion of the (100) facets increases somewhat at ultra low metal loadings since the truncated pyramid structures do not develop further along whiskerettes.

The equilibrium shape and faceting of the PR149-supported metal crystallites are demonstrated in Figure 9A, that is, in the HRTEM image taken of a midsized metal whiskerette. By marking the edges of the facets guided by the phase thickness contrast, as well as after indexing the planes, the above proposed model for a typical whiskerette shape and faceting is self-consistent. Clearly, the predominance of the (111) sites in surface faceting is unique among

(27) Foiles, S. M.; Baskes, M. I.; Daw, M. S. *Phys. Rev. B: Condens. Matter Mater. Phys.* **1986**, *33*, 7983.
(28) Murthi, V. S.; Urian, R. C.; Mukerjee, S. *J. Phys. Chem. B* **2004**, *108*, 11011.
(29) Marks, L. D. *Rep. Prog. Phys.* **1994**, *57*, 603.
(30) Mayrhofer, K. J. J.; Blizanac, B. B.; Stamenkovic, V. R.; Ross, P. N.; Markovic, N. M.; Atanasoski, R. T.; Schmoeckel, A. K.; Vernstrom, G. D.; Debe, M. K. Unpublished work.
(31) Bonakdarpour, A.; Stevens, K.; Vernstrom, G. D.; Atanasoski, R. T.; Schmoeckel, A. K.; Debe, M. K.; Dahn, J. R. *Electrochim. Acta* **2007**, *53*, 688–694.
(32) Debe, M. K. Status and Prospects of PEFC Electrocatalysts: Meeting the Requirements for Automotive Fuel Cells with Nanostructured Thin Film Electrodes. *Proceedings of 3rd International Hydrogen and Fuel Cell Expo Technical Conference*, Tokyo, Japan, Feb. 7–9, 2007; Reed Exhibitions Japan Ltd.: Tokyo, Japan, 2007; FC-8, p 5.
(33) Frank, F. C. In *Growth and Perfection of Crystals*; Proceedings of the International Conference on Crystal Growth, Cooperstown, NY 1958; Doremus, R. H., Roberts, B. W., Turnbull, D.; Wiley: New York, 1958.
(34) Burton, W. K.; Cabrera, N.; Frank, F. C. *Philos. Trans. R. Soc. London Ser. A* **1951**, *243*, 299.

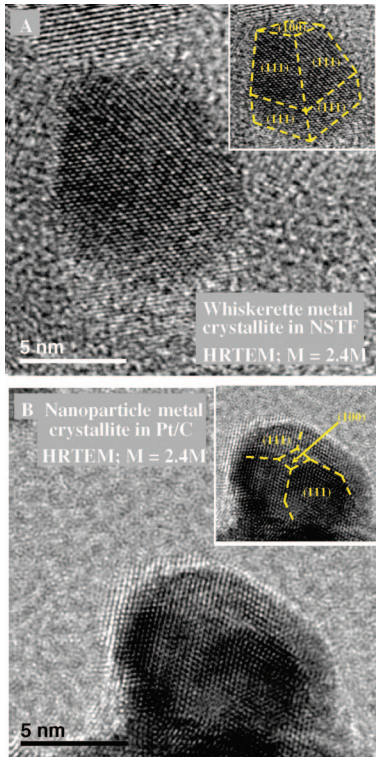

Figure 9. HRTEM images for typical metal crystallites in (A) PR149 whisker-supported NSTF catalysts and (B) a nanoparticle system (Pt black). The insets highlight the faceting.

all nonsupported and supported electrocatalysts. For nonsupported Pt and Pt-alloy crystallites, like those of a single Pt black particle in Figure 9B, many small facets and other steps develop because of the tendency to minimize the cuboctahedron surface energy.[22] At the same time, porous metal structures are formed on conventional carbon supports by ion-beam-assisted deposition (IBAD). However, the structures formed by IBAD on carbon supports lack both a long-range-ordered crystallinity and the well-defined surface morphology.[16]

Parameters of the sputtering conditions used to prepare these NSTF samples are not believed to be responsible for the unique and uniform whiskerette morphology. During sputter deposition preparation of these samples, the substrate was moving relative to the sputtering target causing the angle of deposition to change continuously, and the total metal deposition was achieved through multiple passes under the target. The uniaxial orientation and close spacing of the whiskers presents the opportunity for self-shadowing, which can account for the higher loading on the top parts of the whiskers compared to their bases. The obvious fact that the deposited atoms arrived from the top of the whiskers is also the logical explanation for why the whiskerette axes are oriented uniformly upward, rather than say pointing in a crystallographically equivalent direction toward the whisker base. Beyond that, the metal sputtering deposition conditions applied to prepare the samples for this study are not expected to play any direct role in the development of the unique metal crystallography and uniform surface faceting. Rather, our experimental data imply that the metal whiskerette−crystalline organic whisker interfacial free energy is exceptionally low or that, at the atomic level, there is some epitaxial matching between the PR149 whiskers' crystal lattice structure (bcc (111)) and that of the whiskerett's bases (fcc (111)). Hence, the surface free energy of the metal crystallites as well as surface faceting seem to be strongly influenced by the nature of the PR149 material and the crystal structure.

On the basis of previous electron diffraction study of the PR149 whiskers,[12] it is believed that the bcc face and the side planes are (111) and (011), respectively, with a 14.5(4) Å lattice constant. The whiskerettes, as discussed above, have the fcc lattice structure with a lattice constant of 3.92 Å for pure bulk Pt, and slightly less for the PtRu binary and PtNiFe ternary alloys.[24,35] The model in Figure 8 suggests the fcc (111) planes are in a direct contact with the PR149 whisker bcc (111) side planes, resulting in the observed 70° projection angle. The (111) truncation of the PR149 bcc Bravais lattice would present a hexagonal 2D surface net with surface lattice vectors of $14.5 \times (3)^{1/2} = 25.1$ Å. This surface unit cell diameter of 5.01 nm could accommodate 7.4 of the $3.92 \times (3)^{1/2} = 6.8$ Å Pt fcc (111) surface unit cells, along the major dimensions of the cell. If lattice strain effects constrained this to an integral number of seven Pt unit cell dimensions per one PR149 unit cell dimension, then this could possibly be a mechanism for determining the absolute Pt whiskerette pillar diameter and spacing. The pillar diameter of ~5 nm calculated in this way comes close to the observed pillar diameter of ~6 nm. We must emphasize here that the same structural considerations apply for the PR149-supported PtRu and PtNiFe alloy NSTFs as for the pure NSTF Pt sample. It is furthermore important to note that no evidence for the segregation of the alloying elements was found through our high-resolution energy dispersive spectroscopy studies (not shown).

HRTEM observations and the model proposed in Figure 5A provide a basis to estimate the maximum possible geometric surface area. The roughness factor is estimated for whisker surfaces that carry metal loadings typical of the present work (for the average whisker length of 1 μm). As per ref 12, the rectangular lath-shaped whisker particles have the mean cross-sectional widths of 50 and 25 nm. With the assumption that the whiskerettes are separated by ~6–7 nm from each other, at least 18 of the metal crystallites could be found around a whisker particle on the line perpendicular to the longest axis (3 and 6 on the wide and narrow side planes, respectively). Therefore, one whisker particle of 150 000 nm^2 area holds approximately 2250 whiskerettes in 125 of such zones along the whisker length. (The surface area of the less highly structured tip of the whisker is ignored for this estimate.) If each whiskerette shape is approximated by a square and their pillar axis is allowed to increase gradually from 0 to 25 nm from the bottom to the top of the PR149 whisker, a total of about 900 000 nm^2 of metal surface area can be calculated. This ~6-fold increase in nanoscale roughness per whisker particle can be multiplied by the mesoscale roughness factor of 5–8 given by the typical areal number density of PR149 whiskers of 3–5 billion cm^{-2}.[13] We can then arrive at a nanoscale roughness factor

(35) Stevens, D. A.; Rouleau, J. M.; Mar, R. E.; Bonakdarpour, A.; Atanasoski, R. T.; Schmoeckel, A. K.; Debe, M. K.; Dahn, J. R. *J. Electrochem. Soc.* **2007**, *154*, B566.

(that is the ratio of total surface area compared to the planar or projected surface area) ranging between 27 and 45 for PR149-supported NSTF electrocatalysts. These values are higher by only a factor of 2−3 compared to the typcial electrochemical surface area measured by hydrogen adsorption/desorption at 70 °C on membrane electrode assemblies using similarly prepared NSTF catalysts. Although with a fixed protocol, such surface area measurements are usually good to ±15%, they can easily vary as much as 50% depending on exactly how the area of the cyclic voltammogram is defined or on the temperature and humidity of the measurements. Typically the measured values increase at room temperature as well. More specifically, the surface area is dependent on the loading and in some cases on the particular NSTF alloy and composition used. For example, for the PtNiFe coatings such as seen in Figure 3, the measured electrochemical surface area enhancement factors have been measured as high as 18. This is reasonably close to the calculated estimate above given the range of mesoscale roughness factors and whiskerette number densities assumed for the calculation.

IV. Conclusions

The structure of three compositionally different NSTF electrocatalysts supported on PR149-crystalline organic whiskers was investigated by high resolution transmission electron microscopy. Common trends in the electrocatalyst crystallography, morphology and surface characteristics were observed for NSTF Pt, PtRu, and PtNiFe samples. Specific details of the catalyst particles' growth mechanisms, morphology and support interactions were deduced. The primary findings include the following:

All three catalyst types display a fcc metal crystal structure and exhibit similar morphology to each other on the nanoscale.

The catalyst coating encapsulating the PR149 whiskers consists predominantly of distinct, uniformly oriented whiskerettes, reflecting a unique equilibrium shape in contrast to other nanostructured systems.

The catalyst whiskerettes have different geometric shapes as well as gradually increasing dimensions as their location on the whisker moves progressively from the whisker base to its tip. The fully formed whiskerette crystallites appear as distinct, elongated pyramid-based pillars with cross-sectional dimensions of ∼6 nm. The orientation angle between the whiskerette and whisker axes remains at 70° at all locations on the whisker, being tilted toward the general deposition direction.

A growth mechanism of the whiskerettes over time was deduced from a HRTEM study of the whiskerettes as their development occurs from the base to the tip of the whisker. In the early stage of the crystal growth, at the base of the whisker, the metal atoms arrange into islands on preferential sites of the whisker side planes. The nucleation sites are found on the edge and in the middle of the rectangular lath-shaped whisker side planes, each separated from their neighbors by ∼6–7 nm. A Wulff-construction of a typical Pt based whiskerette shows a pillar having four exposed extended (111) side facets, topped by a pyramid formed by two adjoining smaller (111) and a single (100) facets.

With increasing loading, further up the whisker, they take on a square-truncated pyramid shape. At higher loadings, they form the larger distinct pyramid-based pillars uniformly tilted in two directions in order to maintain the thermodynamic trend of preferential crystal growth along the lowest Miller index single crystal facets. The observed 70° angle between the whiskerette axes and the support whisker's axis is exteremly close to the angles between (111) planes in fcc or bcc lattices, suggesting the size dimensions, uniform orientation, and possibly the natural spacing of the whiskerette pillars are directly related to the epitaxial-like growth of the catalyst onto the whisker's bcc (111) surface planes.

The crystal growth mechanism and morphology of the whiskerettes do not follow a cuboctahedron model of crystal growth because of the exceptionally strong support−metal interactions. Assuming low interfacial free energy between the PR149 support and the Pt pyramid base, only the top side can be truncated by a (100) square plane unlike the case of round nanoparticles on a carbon support. The truncated pyramid shape of the smallest (a few nanometers) metal crystallites is shown to possess the minimum surface free energy.

We conclude that the key difference determining the nanoparticle structure of the NSTF Pt based catalysts and conventional carbon-supported electrocatalysts is the crystalline nature of the PR149 whisker support material. While the PR149 support is not expected to play direct roles in electrocatalysis, its strong influence on the metal whiskerette population density and growth mechanism is evident, in contrast to conventional carbon supports.

Acknowledgment. The authors acknowledge the support under 3M/DOE Cooperative Agreement No. DE-FC36-02AL67621. HRTEM work was carried out at the Center for Microanalysis of Materials of the Frederic Seitz Materials Research Laboratory at Urbana-Champaign. The Wieckowski Group acknowledges partial support by the U.S. Department of Energy, the Grant DOE LANL 53183-001-7.

CM702992B